Journal of Alloys and Compounds 764 (2018) 24–35

Contents lists available at ScienceDirect

Journal of Alloys and Compounds

journal homepage: http://www.elsevier.com/locate/jalcom

Influence of porosity on elastic properties of Ti_2AlC and Ti_3SiC_2 MAX phase foams

Beatriz Velasco [a], Elena Gordo [a], Liangfa Hu [b], Miladin Radovic [b], Sophia A. Tsipas [a, *]

[a] Department of Materials Science and Engineering, IAAB, Universidad Carlos III de Madrid, Avda. Universidad 30, 28911, Leganés, Spain
[b] Texas A&M University, Department of Materials Science & Engineering, College Station, TX 77843, USA

ARTICLE INFO

Article history:
Received 7 February 2018
Received in revised form
15 May 2018
Accepted 3 June 2018
Available online 5 June 2018

Keywords:
MAX phases
Elastic properties
Foams
Ti_2AlC
Ti_3SiC

ABSTRACT

MAX phase foams could have various applications where tailored functional and mechanical properties are required. In this study, Ti_2AlC and Ti_3SiC_2 MAX phase foams with controlled porosity and pore size were produced and characterized. The foams were produced from MAX phase powders by powder metallurgy method using crystalline carbohydrate as a space holder. Foams with overall porosity up to approximately 71 vol% and pore size from 250 μm to 1000 μm were successfully produced; micro-porosity and macro-porosity was characterized. Poisson's ratio and elastic moduli of the foams were measured by resonant ultrasound spectroscopy (RUS) and analyzed as a function of porosity and pore size. Different models were used to fit the experimental data and interpret the effect of pore size and amount of porosity and on elastic properties. It was found that the amount and type of porosity has a larger influence on the elastic properties than the pore size.

1. Introduction

The MAX phases are ternary carbides or nitrides with general chemical formula $M_{n+1}AX_n$ where M is an early transition metal, A is typically an A-group element, X is carbon or nitrogen and n = 1, 2 or 3 [1,2]. MAX phases are considered to be good candidate materials for numerous applications due to their unusual and sometimes unique set of properties [1,2]. As typical metals and alloys, the MAX phases show good damage tolerance and machinability, high thermal and electrical conductivity, and ability to plastically deform more than 25% at high temperatures, even in tension. However, like typical carbides, nitrides and most of other ceramics, they have excellent thermal stability, high stiffness, good corrosion and oxidation resistance, good high-temperature mechanical properties and creep resistance. In addition, they show hysteretic, non-linear elastic stress-strain behavior and can dissipate significant portion of strain energy during cyclic loading even at room temperatures [3–5]. The origin of these unusual properties lies in the nature of their atomic bonds and nano-layered atomic structure [1,2,6].

Over the last two decades, most of the studies have reported on processing, structure and properties of fully dense MAX phases and only a limited number of studies investigated porous ones. Pressureless sintering has been used to produce Ti_2AlC with porosities as low as 10 vol% [7]. Porous Ti_2AlC and Ti_3AlC_2 with up to 80 vol/% porosity, have been also processed using the replication method [8,9]. Most recently, porous Ti_2AlC with porosity up to 93 vol% has been produced by gel casting technique using agarose as a gelling agent to consolidate the foam structure [10]. Reactive sintering of elemental powders in a vacuum furnace has been used to process porous Ti_3SiC_2 with porosity ranging from 28 vol% to 42 vol% [11,12]. This processing method has also been employed to produce porous MAX phase composites of Ti_3SiC_2/TiC, Ti_3AlC_2/TiC, and T_4AlN_3/TiN from various powder mixtures with porosities ranging from 5 vol% to 35 vol% [13]; in another study the same group produced porous 70%Ti_3SiC_2/30%TiC composite by reactive sintering, and demonstrated that porous materials exhibit higher specific strength than fully dense Ti_3SiC_2 [14]. In recent years, the space holder method, adding NaCl particles [15,16] or sugar crystal particles [17,18] has been employed to produce Ti_2AlC [15,17,18] and Ti_3SiC_2 [16] foams, because this method allows not only easy processing of materials with different overall porosity, but at the same time good control of pore sizes.

There is an increasing interest in porous MAX phases with an emphasis on tuning porosity to tailor mechanical properties [7,11,15,19,20] or using them as preforms for composite materials [20–23]. It has been demonstrated that the thermal and mechanical properties of Ti_2AlC and Ti_3SiC_2 decrease with increasing

* Corresponding author.
E-mail address: stsipas@ing.uc3m.es (S.A. Tsipas).

https://doi.org/10.1016/j.jallcom.2018.06.027
0925-8388/

porosity [7,11,15,20]. Previous studies showed that increasing porosity decreases the threshold stresses needed for the formation of kinking bands and subsequently decreases the strength and stiffness of the material [15]. For Ti_3SiC_2 the variation of porosity from 0 vol% up to 55 vol% leads to the decrease of the ultimate compressive strength from 1300 MPa up to 60 MPa respectively [20]; similar tendency is reported for Young's modulus which decreases from 325 GPa to 26 GPa for samples with porosity ranging from 0 vol% up to 55 vol% [20].

In foams, control of pore size and distribution from the processing stage is of outermost importance in order to tailor their final properties. Overall density is the most important parameter affecting elastic properties of the foam [24,25], although Young's moduli of cellular structures are also known to be strongly linked to the architecture of the cellular material [25]. However, there are only few reports on the effects of porosity on the elastic properties of MAX phases, despite the importance it has for structural applications. Young's moduli of porous Ti_2AlC and Ti_3SiC_2 have been reported for porosity up to 40.5 vol% for Ti_2AlC [15] and 55 vol% for Ti_3SiC_2 [20].

This work reports on the effect of porosity on elastic properties of MAX phase foams, namely Ti_2AlC and Ti_3SiC_2. Elastic properties were evaluated not only as a function of porosity but also as a function of pore size distribution. The experimental data were fitted with different existing models over the whole range of porosity. Most existing models used for the prediction of elastic properties only take into consideration limited porosity ranges and do not account for pore size. In this work, experimental elastic properties were fitted over a very wide range of porosity and fitting parameters are related to the microstructure of the porous MAX phases. The technique used in this study to process the foams from the starting MAX phase powders was the space holder technique employing a crystalline carbohydrate as space holder. Different ratios of space holder-powders were selected in order to study the effect of porosity on the properties. Also, different space holder size distributions were introduced in order to study the effect of the pore size on the elastic properties. Characterization of the materials processed with and without space holder included: the phase stability, microstructure and porosity measurements by Archimedes method and image analysis. Elastic properties, namely Young's modulus, bulk modulus and Poisons' ratio, were studied using Resonant Ultrasound Spectroscopy (RUS) and related to the porosity.

2. Materials and methods

In this study two commercial powders were used, namely Ti_2AlC and Ti_3SiC_2 (Kanthal, a Sandvik brand, Sweden) to prepare the MAX phase foams. The particle size distribution of the starting powders was determined to be in: $D_{50} = 9.801\ \mu m$ for Ti_2AlC and $D_{50} = 5.582\ \mu m$ for Ti_3SiC_2 using a Mastersizer 2000 (Malvern Instruments, UK) particle size analyzer.

The powders were mixed with a 2% solution of Acrawax C: $C_{38}H_{76}N_2O_2$ binder (Lonza, Switzerland) to facilitate their compaction. The white sugar powder (Azucarera of AB Sugar, United Kingdom) was used as a space holder. It was first sieved to yield powders with three particle size distributions: 250–400 μm, 400–800 μm and 800–1000 μm. White sugar powders with different size distributions were then mixed with MAX phase powders in three different volume ratios: 0.2, 0.4 and 0.6. This resulted in nine different mixtures of both Ti_2AlC and Ti_3SiC_2 powders using three different volume fractions of white sugar powders, each with three different particle size distributions. The mixtures were then poured inside a silicone mold, sealed and then submerged in the hydraulic oil of a cold isostatic presses (CIP, EPSI, Belgium) and pressed at 400 MPa for 10 min. The green bodies were weighted by a balance with resolution of ±0.0001 g (Mettler Toledo, Spain) to record their mass including the sugar space holder. The green bodies, prior to sintering, were soaked in distilled water at 70 °C for 48 h to remove the space holder. Subsequently, they were dried at 30 °C for 24 h. After the removal of the space holder, the mass of the samples was measured again in order to confirm the completion of the space holder dissolution process. The samples were then sintered in vacuum (10^{-5} mbar) at 1400 °C for Ti_2AlC and 1350 °C for Ti_3SiC_2, for 4 h in a tube furnace (Carbolite, Germany). During heating, all samples were held at 400 °C for 30 min to burn out any space holder residue in the samples. The samples were machined into a cylindrical shape with a lathe to obtain a uniform geometry: a constant diameter along the long direction and parallel bases. Porosity was calculated on machined samples by both Archimedes' principle and measuring the dimensions and mass. The Archimedes' principle was used following the ASTM C20-00 standard and using ethanol to infiltrate the samples and as immersion medium, using procedure described in more detail elsewhere [13,17,18] and using the following equations:

$$\rho = \frac{dry\ mass \cdot \rho_{ethanol}}{wet\ mass - suspended\ mass} \quad (1)$$

$$Porosity_{\ Overall}(\%) = \left(1 - \frac{\rho}{\rho_{teorethical}}\right) \cdot 100 \quad (2)$$

$$Porosity_{open}\ (\%) = \left(\frac{wet\ mass - dry\ mass}{wet\ mass - suspended\ mass}\right) \cdot 100 \quad (3)$$

$$Porosity_{\ closed}(\%) = Porosity_{Overall}\ (\%) - Porosity_{open}\ (\%) \quad (4)$$

where “dry mass” is the mass (in g) of the dry sample, “wet mass” is the mass of the sample after soaking in ethanol during 2 h, “suspended mass” is the mass of the sample suspended in ethanol using a suspending system, $\rho_{ethanol}$ is the density (g/cm^3) of ethanol, $Porosity_{overall}$ is the volume fraction of the overall porosity (vol%) of the sample, $Porosity_{closed}$ is the volume fraction (vol. %) of the closed porosity of the sample and $Porosity_{open}$ is volume fraction of the open porosity of the sample. The density of the starting powder ($\rho_{theoretical}$) was determined by helium pycnometer (Accupyc 1330, Micromeritics, USA).

The phase composition of sintered samples was studied by X-Ray Diffraction (XRD) using X'Pert Diffractometer (Phillips, Holland) with Cu K_α radiation (wavelength = 1.542 Å) at 40 kV and 30 mA in the 2θ range from 8° to 80° with a step size of 0.04° and a step time of 1.5 s. The data was analyzed using Inorganic Crystal Structure Database (ICSD) and Powder Diffraction File (PDF-2) database**.** The phase stability was studied by doing XRD analysis in three conditions of the material: raw powder, sintered with and without space holder. The molar fraction of the phases was calculated by the relationship of I_x/I_t where I_x is the integrated intensity of highest representative peak of each phase and I_t is sum of the integrated intensities for the highest representative peaks of all the constituent phases of the material. The mass loss after sintering expresses the mass variation of the green body compared to that in the sintered state.

The samples were cut, mounted in resin, and then ground and polished with 1 μm diamond abrasive for metallographic observation. The microstructural images were obtained by a scanning electron microscope (SEM; Philips XL-30, with filament of W) using the accelerating voltage and emission current of 15 kV and 20 mA, respectively.

Image analysis was performed on SEM images using image-j

software. For each foam, the image analysis was performed following the ASTM E112-12 standard on at least 3 images from three different areas. For samples with bigger space holder size range (800–1000 μm) the entire cross section was analyzed due to the limited number of pores in each image. Magnification of 2500× was used to study the porosity within the struts in the foam and magnification of 65× to study the porosity introduced by the space holder. The equivalent circular diameter (EDC) as the diameter of an equivalent circle with the same area as the pore cross-section area was calculated using the following equation [26]:

$$ECD = \sqrt{\frac{4A}{\pi}} \quad (5)$$

where A is the pore area. The ECD was determined for each pore in different foams. The median value of the ECD, for each sample was determined as the value at the cumulative frequency of 50%.

The elastic properties and Poisson' ratio were determined by resonant ultrasound spectroscopy (RUS; Magnaflux Quasar Systems, NM) using procedure described in more detail elsewhere [15,27,28]. The collected resonant spectra were analyzed using Quasar RuSpec software (Magnaflux Quasar Systems, NM) that iteratively calculates resonate peaks of the isotropic sample assuming different values of elastic constants (C11 and C44), until they converge closely the measured resonant frequencies of the sample with known geometry and mass. The criterion for accepting the determined elastic constants through described iterative process was a root-mean-square error (RMSE) between calculated and measured positions of resonant peaks below 0.50%.

3. Results

3.1. Microstructural characterization and porosity measurements

The phase composition of the starting material and the processed foams was investigated by XRD. XRD results in Fig. 1a show that the starting Ti_2AlC powder contains two major phases (Ti_2AlC and Ti_3AlC_2) and two minor phases (TiC and Al_2O_3). The same phases were identified in the sintered samples with and without space holder and agree with the phases commonly observed in this material. The molar fractions of identified phases determined from XRD results are shown in Table 1. There is a slight decrease of the amount of Ti_2AlC after sintering in both cases, with and without space holder.

Fig. 1b shows the XRD results for the Ti_3SiC_2. The initial powder contains Ti_3SiC_2 as the major phase and TiC as the minor phase. No other phases were identified by the XRD neither in the material sitnered using space holder nor in the material sintered without using space holder. Table 2 shows the molar fractions of the phases identified in the Ti_3SiC_2 samples. After sintering, no difference in the molar fractions of the phases can be observed for the sample without space holder. For the sample sintered using 60 vol% space holder, the amount of TiC phase increases 16% after sintering. In order to investigate the origin of observed phase changes in those samples, the mass loss during sintering of the Ti_3SiC_2 foam was monitored and results are summarized in Fig. 2. It is clear from Fig. 2 that mass loss increases from 3.69% to 6.84% as the volume of space holder increases from 0 vol% to 60 vol%.

Overall, open, and closed porosities in all processed foams were determined using Archimedes' method and results are summarized in Fig. 3 for both Ti_2AlC (Fig. 3a–d) and Ti_3SiC_2 (Fig. 3e–h) foams with different volume fractions of the space holder. Note that results in Fig. 3 also show overall, open and closed porosities in samples sintered without using any space holder at the same sintering conditions. In addition, the overall theoretical porosity is compared to the experimental one for the three space holder with different particle size ranges in Fig. 3d and h for both Ti_2AlC and Ti_3SiC_2 foams, respectively. The theoretical porosity was calculated assuming that the overall porosity is equal to volume fraction of the space holder used during processing.

Fig. 3a-c show that Ti_2AlC samples sintered without space

Table 1
Comparison of the molar fractions of the four phases for the Ti_2AlC material in three different conditions: raw powder, sintered with 0 vol% space holder and with 60 vol % space holder.

Phase	Molar fraction (%)		
	Raw	Sintered	Sintered
	Powder	0 vol% space holder	60 vol% space holder
Ti_2AlC	63	59	54
Ti_3AlC_2	25	31	29
TiC	6	5	9
Al_2O_3	6	5	8

Table 2
Comparison of the molar percentages (%) of the phases for the Ti_3SiC_2 material in three different conditions: raw powder, sintered with 0 vol% space holder and with 60 vol% space holder.

Phase	Molar fraction (%)		
	Raw	Sintered	Sintered
	Powder	0% SH	60% SH
Ti_3SiC_2	79	79	63
TiC	21	21	37

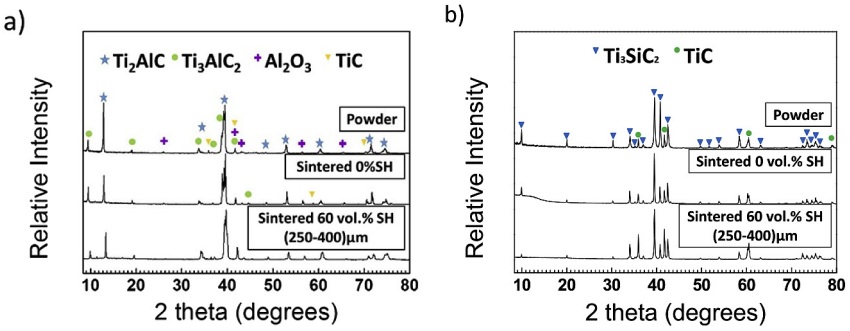

Fig. 1. XRD results of the raw powder, sintered material without space holder and with 60 vol% space holder for a) Ti_2AlC and b) Ti_3SiC_2. The identification is performed using Inorganic Crystal Structure Database (ICSD: 165460 for Ti_2AlC, 153266 for Ti_3AlC_2, 10425 for Al_2O_3, and 44495 for TiC) and to the Powder Diffraction File (PDF-2: 01-074-0310 for Ti_3SiC_2 and 03-065-0242 for TiC).

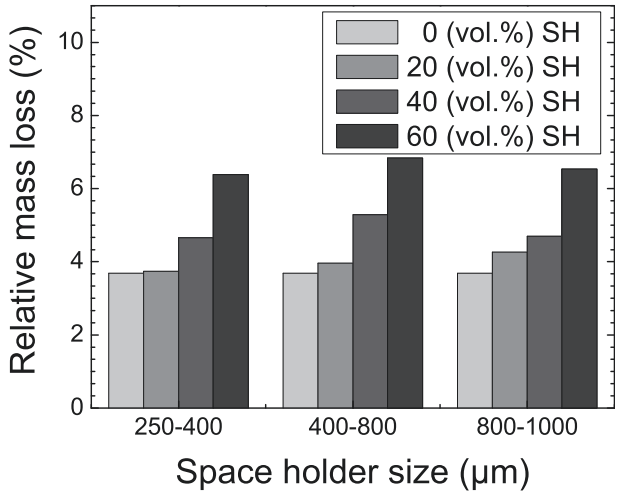

Fig. 2. The mass loss (%) during sintering of the Ti_3SiC_2 material with three volume ratios of space holder (20 vol%, 40 vol% and 60 vol%) and three space holder size ranges (250–400 μm, 400–800 μm and 800–1000 μm) in comparison with the material without space holder.

holder have 10% of mostly closed porosity. Those pores are around a micron-size (Fig. 4e and f) and appear not only in the samples sintered without using space holder, but also in the struts of all foams processed using different volume fractions of space holder. For samples processed using 20 vol% or more of space holder, overall porosity (P) is always larger than open porosity (P_{open}), which is, in turn, always larger than closed porosity (P_{closed}), i.e. $P > P_{open} > P_{closed}$. While closed porosity remains always below ~20 vol% and decreases with amount of space holder, open porosity increases with amount of space holder, regardless of space holder size range. Ti_3SiC_2 samples without space holder show around 31% porosity, Fig. 3e-g. The porosity is mainly open and $P > P_{open} > P_{closed}$. The open porosity increases with increasing amount of space holder regardless of the space holder particle size range.

Fig. 3d and h show the differences between experimental and theoretical porosities. For samples with 0 vol% of space holder, the difference between measured and theoretical porosity is higher for Ti_3SiC_2 than for Ti_2AlC, because of higher incomplete densification of the samples during presureless sintering. For samples processed with 40 vol% of space holder or more, the measured porosity is close to the theoretical one.

For Ti_2AlC, experimental and theoretical porosities are very close to each other, suggesting that most of the porosity is generated by the space holder. Ti_3SiC_2 samples show a larger difference between experimental and theoretical porosity due to the fact that the foam cell walls (or struts) in Ti_3SiC_2 contain more micron-sized pores than in Ti_2AlC foams. For both materials, experimental porosity tends to be closer to the calculated one as the amount of space holder increases. This occurs because relative contribution of porosity from cell walls (micrometer-sized pores) decreases with increasing macro porosity introduced by the space holder.

Fig. 4e and f shows selected but typical images of the microstructure of the cell walls (or struts) in Ti_2AlC and Ti_3SiC_2 foams. Both materials have micron-sized pores that are homogeneously distributed in the cell walls, but Ti_3SiC_2 foams contain a larger amount of those pores (Fig. 4e and f) than Ti_2AlC foams.

The millimeter-sized pores (macro pores) introduced by the space holder (Fig. 4c and d) replicate the space holder's shape. The porosity is randomly and homogeneously distributed. Similar size and amount of porosity is achieved in both materials with the same volume percent and particle size range of space holder. Photographs of the foams are also shown in Fig. 4a and b, for Ti_2AlC and Ti_3SiC_2 foams, respectively. The foams have been machined to a cylindrical shape in order to perform RUS measurements. The homogeneity and integrity of all foams is evident, including the foams with the highest amount of space holder.

The Equivalent Circular Diameter (ECD) of micron-sized pores in the cell walls was determined to better understand the influence of the space holder on their size (Fig. 5). The ECD of micron-sized pores was found to be in ~1.5 μm in both Ti_2AlC and Ti_3SiC_2 samples. Results in Fig. 5 indicate that addition of space holder does not affect the size of micron-sized pores, i.e. it barely changes with increasing both volume fraction and particle size of space holder. These results show that the micron-sized pore size is insensitive to the size and amount of space holder, and confirm that they are formed as a result of incomplete deification during presureless sintering.

Fig. 6 shows the porosity determined by analysis of SEM images of Ti_2AlC and Ti_3SiC_2 foams processed using space holder with 250–400 μm particle sizes. Note that results in Fig. 6 are provided for micron-sized pores in the cell wall and for macro pores introduced by the space holder. Results in Fig. 6 agree in general with the trends observed from measurements using Archimedes' method (Fig. 3), with a difference in porosity between two different measurement methods of 0.4 %–7% for Ti_2AlC and 1%–11% for Ti_3SiC_2. For both Ti_2AlC and Ti_3SiC_2, results in Fig. 6 once again confirm that the amount of macro pores increases almost linearly as the amount of space holder increases, although it is always slightly lower than the volume fraction of the space holder used in foam processing. The amount of micro-sized pores decreases as the amount of space holder increases (Fig. 6), which is also consistent with previous results in Fig. 3.

3.2. Elastic properties

The elastic properties were measured for all samples, including foams with porosity as high as 71 vol%. Note here that all processed foams were strong enough to be handled and machined successfully into cylindrical samples with high dimensional precision that is needed to perform reliable RUS testing. Figs. 7 and 8 show Young's (E) and shear (G) moduli of Ti_2AlC and Ti_3SiC_2 foams, respectively, determined by RUS as a function of porosity. For comparison, Figs. 7 and 8 also show elastic moduli of fully dense Ti_2AlC and Ti_3SiC_2 previously published in literature [7,29], as well as those previously reported for porous samples manufactured by SPS [15,29], HIP [20] and space holder method with NaCl [15].

The experimental data obtained in this study (Figs. 7 and 8) have been fitted using four different models, namely exponential model [30,31], Hasselman model [32], composite sphere model (CSM) [33–35] and the percolation model [36–38]. Note that for performing the fitting, the values for the fully dense materials were taken from previously published results [7,29]. The expressions used in each case are given below:

Exponential model [30,31]:

$$\frac{E}{E_0} = \frac{G}{G_0} = e^{-a \cdot P} \tag{6}$$

Hasselman model [32]:

$$\frac{E}{E_0} = \frac{G}{G_0} = 1 - \frac{aP}{1 + (a-1)P} \tag{7}$$

Composite Sphere model (CSM) [33–35]:

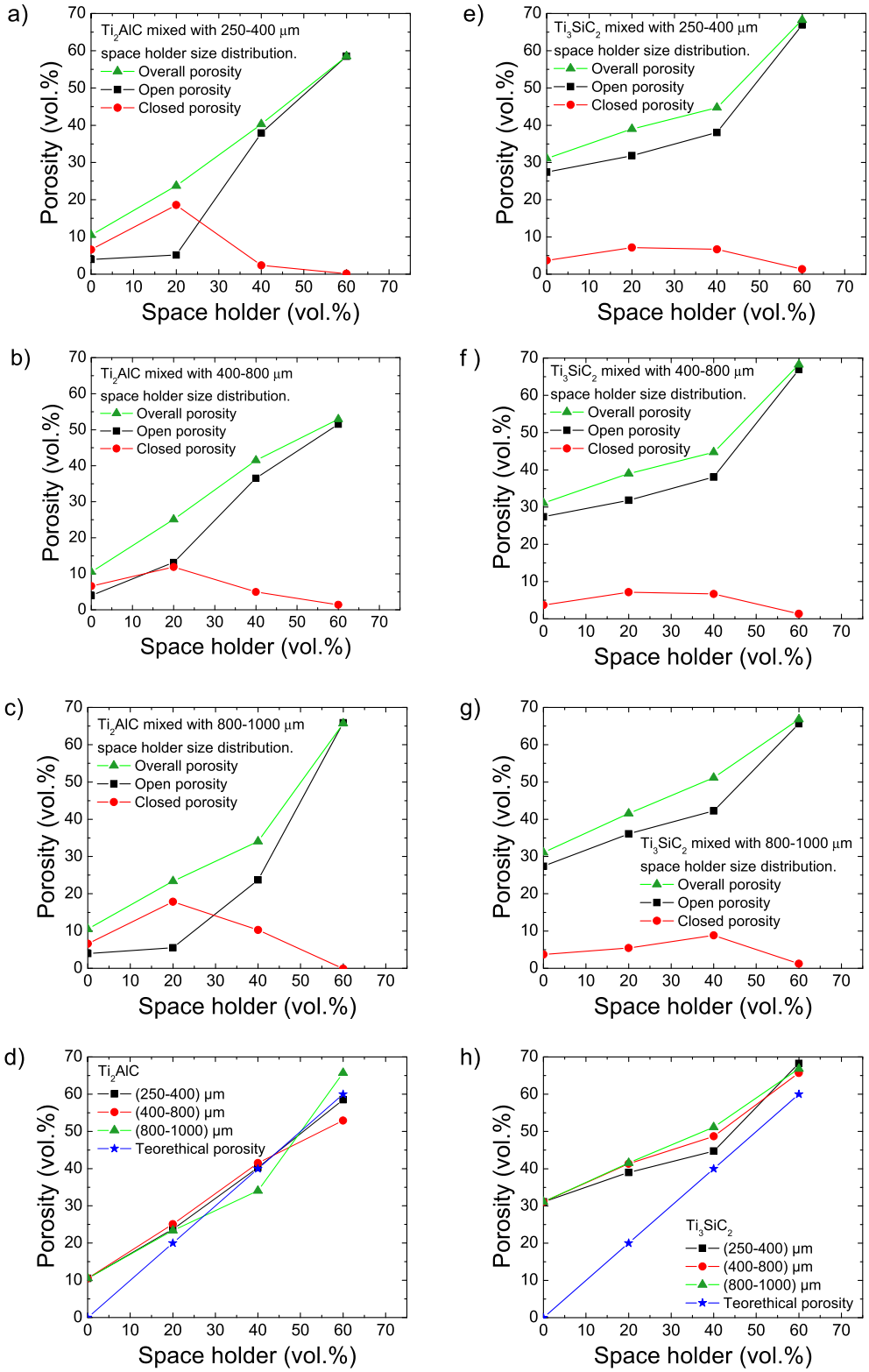

Fig. 3. Overall, open and closed porosity mesured by Archimedes' method for different space holder size ranges.; a) Ti_2AlC foams with 250–400 μm, b) Ti_2AlC 400–800 μm, c) Ti_2AlC 800–1000 μm, e) Ti_3SiC_2 250–400 μm, f) Ti_3SiC_2 400–800 μm, g) Ti_3SiC_2 800–1000 μm. Comparison between theoretical and experimental porosity for: d) Ti_2AlC and h) Ti_3SiC_2 with three space holder size ranges.

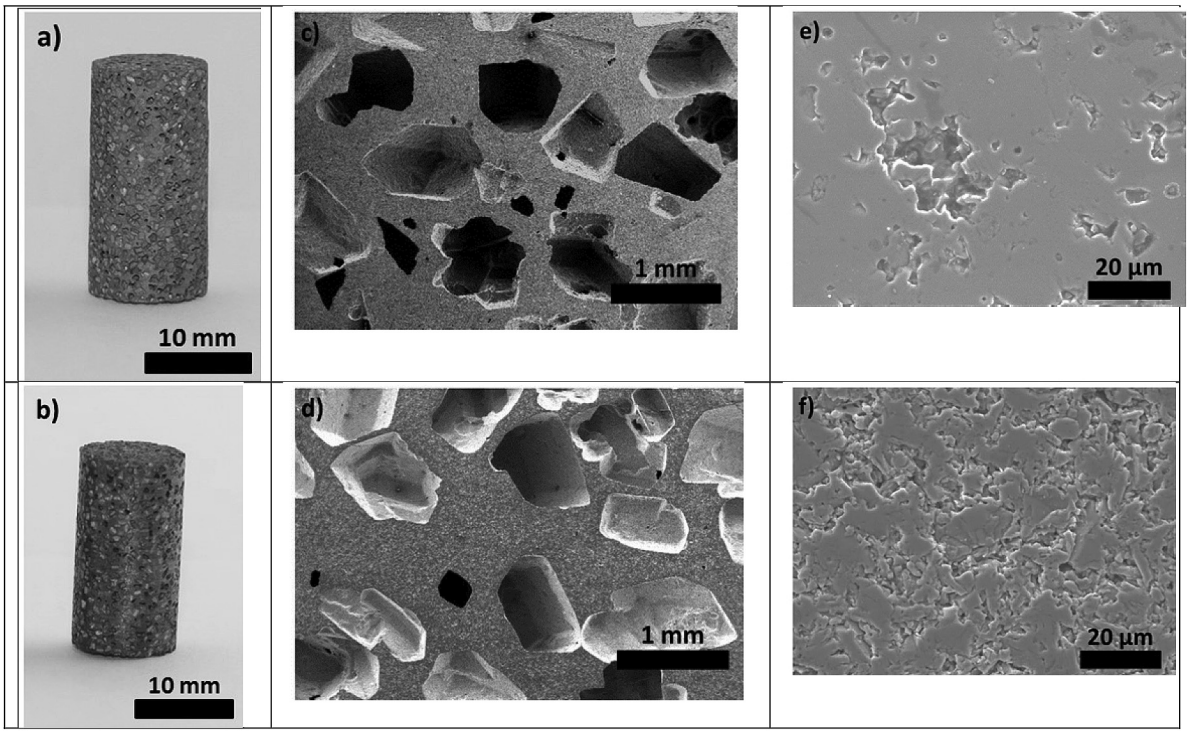

Fig. 4. Representative images of foams of both materials containing 60 vol% space holder and with 800–1000 µm space holder size distribution in three different magnifications: a) macrophotograph of Ti_2AlC foam, b) macrophotograph of Ti_3SiC_2 foam; c) characteristic SEM image of the microstructure of Ti_2AlC foam d) characteristic SEM image of the microstructure of Ti_3SiC_2 foam; e) cell-wall of Ti_2AlC foam and f) cell-wall of Ti_3SiC_2 foam.

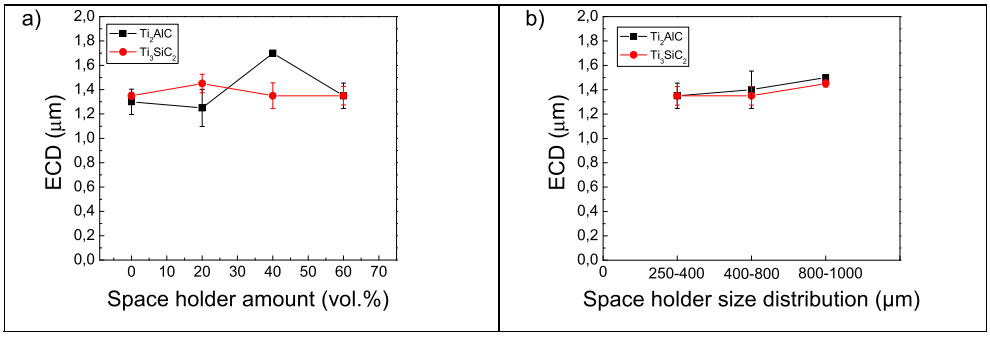

Fig. 5. Median value ECD (µm) of the micrometer-size pores for the materials Ti_2AlC and Ti_3SiC_2 with respect to a)space holder volume fraction (for space holder size 250–400 µm) and b) size ranges (for 60 vol% space holder).

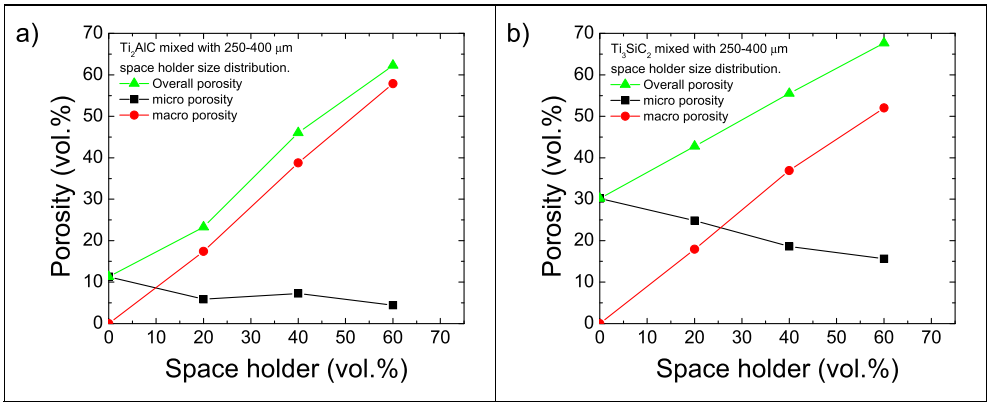

Fig. 6. Porosity mesured by image analysis for micron-size and macro pores in a) Ti_2AlC and b) Ti_3SiC_2 foams, both processed using space holder with 250–400 µm particle size.

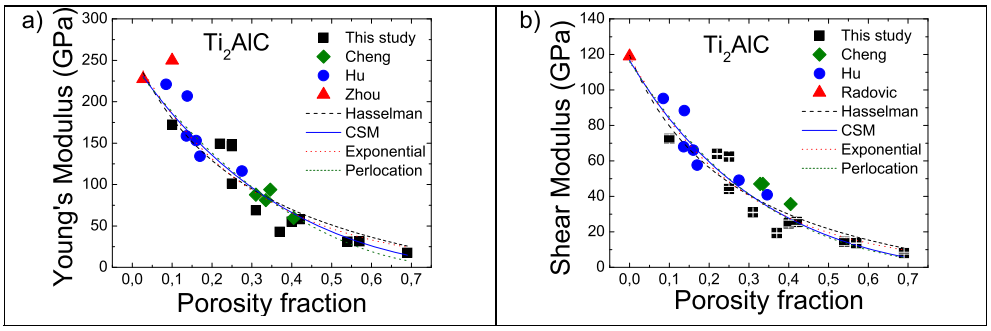

Fig. 7. Variation of a) young's modulus and b) shear modulus elastic properties of Ti_2AlC with porosity in comparison to data previously published by Cheng [39], Hu [15] Zhou [7] and Radovic [29]. Solid, dotted and dashed lines are results of fitting using exponential [30,31], Hasselman [32], CSM [33–35] and the percolation [36–38].

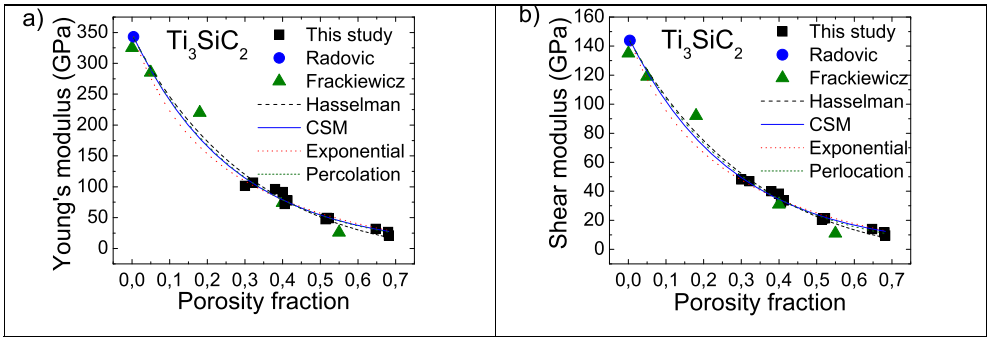

Fig. 8. Variation of a) young's modulus and b) shear modulus elastic properties of Ti_3SiC_2 with porosity in comparison to data previously published by Fraczkiewicz [20] and Radovic [29]. Solid, dotted and dashed lines are results of fitting using exponential [30,31], Hasselman [32], CSM [33–35] and the percolation [36–38] models.

$$\frac{E}{E_0} = \frac{G}{G_0} = \frac{(1-P)^2}{1-aP} \tag{8}$$

Percolation model [36–38]:

$$\frac{E}{E_0} = \frac{G}{G_0} = (1-aP)^n \tag{9}$$

where E_0 and G_0 are the Young's and the shear moduli of fully dense material, respectively, P is overall porosity, and a and n are constants. In the CSM model, the constant a depends on the modulus and is a function of Poisson's ratio of the corresponding dense solid [34]. For the percolation model, a can be defined as $a = 1/P_c$, where P_c is the porosity at which the effective modulus becomes equal to zero. The constant n depends on the materials properties and porous microstructure. The minimum value of a for the percolation model is *1* corresponding to a $P_c = 1$.

The results of the fitting using all four models (Equations (6)–(9)) are summarized in Tables 3 and 4, together with the coefficient of regression R^2. The experimental data of this study were compared to those found in literature for Ti_2AlC and Ti_3SiC_2 foams. The data of elastic properties of foams from literature plotted in Figs. 8 and 9 for comparative purpose corresponds to foams that were manufactured in different ways including SPS [15,29], HIP [20] and space holder method with NaCl [15] and hence resulted in foams with different pore morphology and pore size. The data for fully dense materials from the literature are as following: Young's moduli of 277.6 GPa [7] and 343 GPa [29] for Ti_2AlC and Ti_3SiC_2 respectively and the shear modull of 118.8 GPa [29] and 143.8 GPa [29] for Ti_2AlC and Ti_3SiC_2 respectively.

Figs. 9 and 10 show variations of E and G with porosity, for Ti_2AlC and Ti_3SiC_2 foams, respectively, processed using space holder with different particle size ranges, together with results of fitting using CSM model.

Fig. 11a shows the Poisson's ratio determined for porous Ti_2AlC together with the values found in literature for samples produced using with different techniques [6,15,29,40]. The different pore sizes don't show a clear tendency in the behavior. Fig. 11b shows the variation of Poisson's ratio with porosity for Ti_3SiC_2. Both materials show that Poisson's ratio decreases slightly with porosity.

4. Discussion

4.1. Phase stability

The results presented in this paper show clearly that soluble

Table 3
Result of fitting data in Fig. 7 for Ti_2AlC, using exponential [30,31], Hasselman [32], CSMS [33–35] and percolation [36–38] models.

Model	E				G			
	A	E_o	n	R^2	a	G_o	n	R^2
Exponential	3.4 ± 0.4	260 ± 22	–	0.89	3.6 ± 0.3	119 ± 8	–	0.92
CSM	0.9 ± 0.5	249 ± 22	–	0.90	1.3 ± 0.5	117 ± 8	–	0.93
Hasselman	4.1 ± 1.0	262 ± 29	–	0.88	4.5 ± 0.8	119 ± 9	–	0.91
Percolation	1.1 ± 0.5	245 ± 22	2.2 ± 1.4	0.90	1 ± 0.7	116 ± 8	3.2 ± 2.9	0.92

Table 4
Result of fitting data in Fig. 8 for Ti_3SiC_2, using exponential [30,31], Hasselman [32], CSMS [33–35] and percolation [36–38] models.

Model	E				G			
	a	E_o	n	R^2	a	G_o	n	R^2
Exponential	3.7 ± 0.1	348 ± 7	–	0.99	3.6 ± 0.1	147 ± 2	–	0.99
CSM	1.4 ± 0.2	346 ± 9	–	0.99	1.2 ± 0.1	145 ± 3	–	0.99
Hasselman	5.1 ± 0.3	351 ± 8	–	0.99	4.9 ± 0.2	147 ± 3	–	0.99
Percolation	1.0 ± 0.3	342 ± 15	3.1 ± 1.4	0.97	1.0 ± 0.3	144 ± 5	3 ± 1	0.98

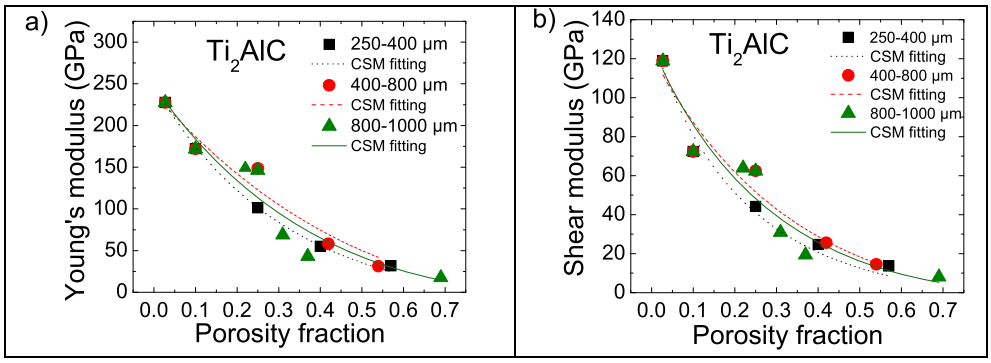

Fig. 9. Variation of a) E and b) G with porosity for Ti_2AlC using three space holder size ranges: 250–400 μm, 400–800 μm and 800–1000 μm and fitting for the composite sphere model [33–35]. For fully dense materials the data has taken from the literature: Young's modulus 277.6 GPa [7] and shear modulus: 118.8 GPa [29].

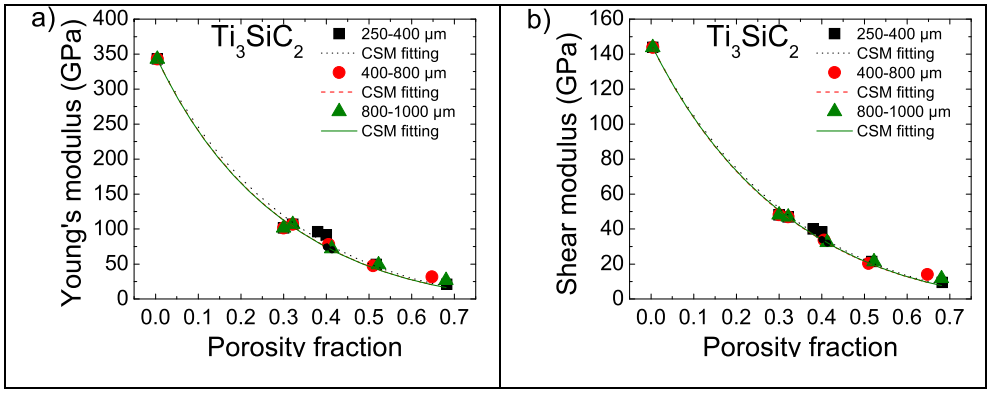

Fig. 10. Variation of a) E and b) G with porosity for Ti_3SiC_2 employing three space holder size ranges: 250–400 μm, 400–800 μm and 800–1000 μm and fitting for the composite sphere model [33–35]. Young's modulus: 277.6 GPa [7] and the shear modulus: 118.8 GPa [29]. For fully dense materials the data has taken from the literature: Young's modulus: 343 GPa [29] and shear modulus: 143.8 GPa [29].

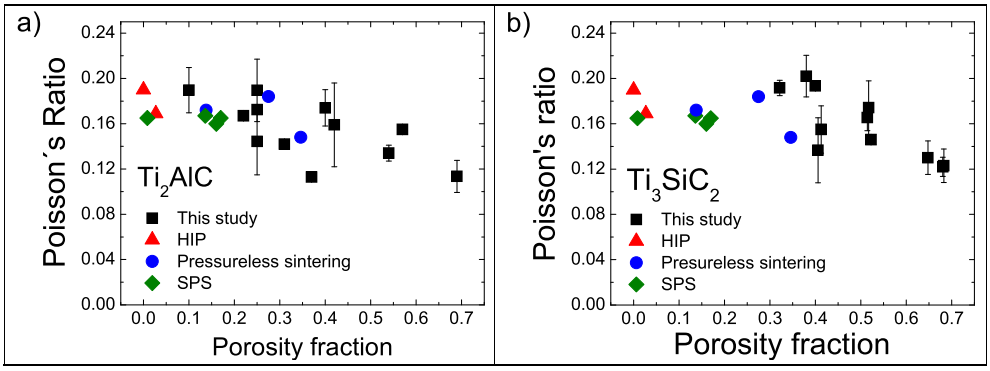

Fig. 11. Experimental results of Poisson's ratio versus porosity for: a) Ti_2AlC and b) Ti_3SiC_2 and comparison with the published by HIP [6,40], Pressureless sintering [15] and SPS [29].

crystalline carbohydrate can be used for easy processing of T_2AlC and Ti_3SiC_2 foams with up to 60% porosity and tailoring pore sizes and thus elastic properties of MAX phase foams. For both Ti_2AlC and Ti_3SiC foams, slight compositional differences can be observed between the as-received powders, the sintered powders without space holder and the foam materials, as it is shown in Fig. 1 and Table 1. These compositional differences could be attributed to decomposition of the MAX phase powders during the sintering process and in the case of the foams, they could also arise due to reaction of the powder with space holder residues. During foam production using a leachable space holder material, incomplete removal of the space holder due to incorrect elimination might cause undesirable phase changes. A complete de-binding process is therefore essential to prevent formation of any undesired phases as result of the reaction between powder and space holder material or binder.

For the Ti_2AlC foams, there are small differences in the phase composition between the samples sintered with and without space holder with respect to the starting powder (Fig. 1a and Table 1). These phase changes observed are most probably a result of the higher amount of surface area in the material with space holder, and not a consequence of the reaction of between the Ti_2AlC with and any C from space holder residues. In previous studies on the phase stability of Ti_2AlC foams [17] the phase changes observed were attributed to the sintering cycle. The phase changes observed in this study are consistent with the phase changes reported in literature for this material during sintering. It can be observed that a higher amount of Al_2O_3 phase is present in the material with space holder as a result of oxidation in the foam during sintering, attributed to a higher amount of surface area in the foam. It has been established that at temperatures above 1400 °C in vacuum, Ti_2AlC is susceptible to decomposition through sublimation of Al and Ti to form TiC by the following reaction [41,42]:

$$Ti_2AlC_{(solid)} \rightarrow TiC_{(solid)} + Ti_{(gas)} + Al_{(gas)} \quad (10)$$

Since sintering was performed in vacuum and the surface area of the foam material is bigger that the material without space holder, this probably accounts for the higher amount of TiC and Al_2O_3 observed, as opposed to the material sintered without space holder. In addition, an increase in the amount of Ti_3AlC_2 is observed in both samples sintered with and without space holder. It has been reported that Ti_2AlC can transform to Ti_3AlC_2 at high temperatures probably through the following reaction [43]:

$$2Ti_2AlC_{(solid)} \rightarrow Ti_3AlC_{2\,(solid)} + TiAl_{(1-x)\,(liquid)} + xAl_{(gas)} \quad (11)$$

The amount of $TiAl_{(1-X)}$ is almost impossible to detect by x-ray diffraction due to its nonstoichiometry and small amount [43].

Regarding the phase transformations observed in the Ti_3SiC_2 foams, previous studies on the phase stability of Ti_3SiC_2 reported that Ti_3SiC_2 can decompose starting from 1000 to 1400 °C in vacuum [44–48]. However, El-Raghy and Barsoum [49] showed that Ti_3SiC_2 was thermodynamically stable up to 1600 °C in vacuum furnace for 24 h. The decomposition at lower temperatures can be caused by small amount of impurities in the starting powder [50]. Previous studies have reported that carbon impurities in porous samples led to the formation of TiC_x and vaporization of Si according to the following reaction [51]:

$$Ti_3SiC_{2\,(solid)} + (3x-2)C_{(solid)} \rightarrow 3TiC_x(x > 0.8)_{(solid)} + Si_{(gas)} \quad (12)$$

In order to verify that the decomposition of the Ti_3SiC_2 occurs partly due to vaporization of Si according to reaction 12, the mass loss during sintering was measured (Fig. 2). For the sample without space holder there is a total mass loss of about 3.69%, including the mass loss due to de-binding of the pressing lubricant, which is 2%. The mass loss during sintering suggests that the vaporization did indeed occur during sintering, regardless of the presence of space holder. The mass loss increases with porosity since the increasing specific surface area favors the removal of Si vapor. This result is consistent with that reported by El Raghy and Barsoum [51]. For the samples with 0% and 60% space holder, the measured molar percentages of TiC after sintering were 21% and 37%, respectively (Table 2). This means that no phase changes are observed for 0% of space holder, whereas a 16% increase in TiC molar percentage for 60% space holder samples is noted. Assuming that all measured mass loss is due to the Si vaporization according to equation (12), the hypothetical increment in TiC phase was calculated for the samples with 0% and 60% of space holder and compared with the observed TiC molar percentage. Comparing the measured mass loss with the increment in TiC phase there was a good agreement with only a difference of 1% and 2% in TiC amount for samples with 0% and 60% of space holder, respectively. This suggests that the mass loss and phase changes are due to the Si evaporation according to reaction 12. On the other hand, the amount of C necessary for a 16% increase in TiC molar percentage according to reaction 12 is 125% larger than the total C present in the space holder used and three orders of magnitude larger than any residual C in the sample. Hence, the reaction of Ti_3SiC_2 with C to form TiC according to equation (12) is most likely not the only mechanism responsible for the phase changes observed. Therefore, the phase changes are more likely due to the Si vaporization favored by the increasing specific surface area and are not a result of reaction with C residue.

4.2. Effect of porosity on elastic properties

In the present study elastic properties were determined for samples with porosity ranging from 10 vol% to 71 vol% for Ti_2AlC and 30 vol% to 69 vol% for Ti_3SiC_2. To the best of our knowledge, no measurements of the elastic properties have been reported before for porosity values higher than 40.5 vol% for Ti_2AlC and 55 vol% for Ti_3SiC_2. Four different models have been fitted to the experimental data, namely exponential [30,31], Hasselman [32], CSM [33–35] and the percolation [36–38] models. Fitting of elastic properties of porous materials over a wide range of porosities with a single equation is usually challenging since an increase in porosity is often accompanied by a change in microstructure or type and shape of pores, for example a change from closed to open porosity as porosity increases. Different fitting models usually are derived assuming specific microstructural characteristics and therefore cannot be used to describe accurately change in elastic properties in a wide porosity range if it is accompanied by changes in the microstructure. All above mentioned existing models are developed for porosity up to approximately 38 vol% [52].

The exponential model has been cited extensively for predicting elastic properties of porous materials; however, it is an empirical model that fails to satisfy the boundary condition that the Young's modulus must be equal to zero when porosity is 100 vol%. In addition, this model is only accurate for a narrow range of porosities, i.e., lower that 20 vol%. Hasselman model is based on the assumption that a continuous phase contains a dispersed phase of spherical particles – in this case the dispersed phase consists of pores and thus the elastic properties of the pores are considered to be equal to zero. This model satisfies the boundary conditions and can be used for a wider range of porosities. The CSM considers an assembly of hollow spheres, of different diameters but the same porosity fraction of each cluster of hollow spheres, using the principle of statistical continuum mechanics. The percolation model is based on the percolation theory and the material constant

a is the percolation threshold. Therefore, the minimum value of a is $a \geq 1$ for a maximum porosity of 100 vol%. The percolation threshold is a function of powder size, shape and distribution [36–38].

For Ti_2AlC the model that fits better with the experimental data is the CSM model, since it has the slightly higher coefficient of determination, R^2, for both Young's and shear moduli (Table 3). CSM model assumes that the material is isotropic with homogeneous distribution of porosity, which coincides with the main observed microstructural features of the foams. Regardless of that, taking into account that R^2 for Young's and shear moduli (Table 3) varies between 0.89-0.90 and 0.91–0.93, respectively, one can conclude that all four models can be used equally well to describe changes of elastic properties with porosity. The values for E_o given by the models are slightly lower in all cases than the experimental values for the dense material (277.6 GPa [7]), whereas the values for G_o are very close to the experimentally measured values (118.8 GPa [29]). The percolation model for the Young's modulus gives a value for the constant a of *1.1*, which corresponds to a percolation threshold value of $P_c = 0.91$. Therefore, for a porosity of 91 vol%, the Young's modulus should reach zero according to that model. The elastic properties from literature for porous Ti_2AlC are also in good agreement with results presented in this study [7,15,39] (Fig. 7).

For Ti_3SiC_2, all models present a good fit of experimental data with values for the coefficient of determination, R^2 exceeding 0.97 (Table 4). All Ti_3SiC_2 foams have an open cell structure (Fig. 3 e–g), and thus the description of the variation of the elastic properties over the whole porosity range with a single equation is more reasonable as there is no change in the type of porosity and foam morphology. The values for E_o given by the all models are close to the experimental values for the fully dense material of 343 GPa [29]. Similarly, for all models the values for G_o are also very close to the experimentally measured value of 143.8 GPa [29] for fully dense samples. The value of the constant a in the percolation model is 1 and that implies that the elastic constants become zero for a porosity of 100 vol%. Data from Fraczkiewicz [20] follow a similar trend in comparison to the experimental data obtained in this study (Fig. 8).

For Ti_2AlC (Fig. 9), higher values of E, G and B are achieved for bigger space holder sizes for porosities in the range of 0–25 vol%. Examining the type of cell structure for this porosity range (Fig. 3 a–c), we found that for bigger space holder sizes, foams with low porosity up to 25 vol% have mainly a closed cell structure. It is well established that the linear elastic behavior of porous solids depends largely on whether the cells are open or closed [24]. If the cell walls are relatively thin, elastic moduli of closed cell porous structures are identical to those of an open cell foam. However, if this is not the case, the cell edges can strengthen the structure due to the limited deformation mechanisms compared to the open structure, resulting in more rigid structures and higher E, G and B values. As porosity increases, the differences in the elastic properties for foams with different pore sizes become less significant. For larger porosity values, cell structure is mostly open for all pore sizes, hence the deformation mechanism is similar for all foams, regardless of pore sizes. For Ti_3SiC_2, all the foams in this study had an open cell structure (Fig. 3 e–g). Therefore, the rigidity/elasticity of the structure is not altered significantly with increasing porosity. Fig. 10 shows no significant differences in the elastic properties for different space holder size ranges.

Microstructural observation of the foams (Fig. 4) reveals that they are characterized both by microporosity and macroporosity. The starting powder particles have angular shape, with high specific surface and with a relative narrow powder particle size distribution. Powders with such characteristic generate a bimodal porosity after sintering: micro-sized pores in the cell walls of the structure (microporosity) and macro-pores (macroporosity) generated by the removal of the space holder.

Ti_2AlC samples without space holder have 10% porosity, and this porosity is mainly closed. Ti_3SiC_2 samples without space holder show around 31% porosity, which is mostly open. In both cases, the micro-sized pores are present when no space holder is introduced because of incomplete sintering. The average size of the microporosity, estimated using the equivalent circular diameter (ECD) is 1.2–1.8 μm for Ti_2AlC and 1.3–1.5 μm for Ti_3SiC_2 (Fig. 5). As it is evident in Fig. 5, the size of the ECD of the microporosity is not affected significantly by either the space holder amount (Fig. 5a) or the space holder size distribution (Fig. 5b). The later confirms that micro-porosity is result of incomplete sintering of the struts in the MAX phase foams.

On the other hand, from Fig. 6 it can be seen that the amount of microporosity decreases almost linearly with increasing amount of space holder for both materials, whereas the amount of macroporosity increases. This is because microporosity is present only in the cell walls, and thus the relative contribution to porosity from cell walls decreases as the overall porosity increases. In addition, when considering the amount of open and closed porosities, it can be observed that the amount of open porosity increases with increasing amount of space holder regardless of space holder size distribution (Fig. 3). These results suggest that as the overall porosity increases, regardless of pore size, the cell walls become thinner and the microporosity becomes interconnected and contributes to the total amount of open porosity. However, the type of porosity, in terms of open or closed porosity, has a more significant influence on the elastic properties than the presence and amount of micro-porosity, or the size of macro-pores.

Fig. 11 presents the experimental results of Poisson's ratio with respect to porosity for both materials in comparison to the literature values [6,15,29,40] from different methods. The differences of the values obtained for each porosity percentage are considerable, and thus it is difficult to establish a trend. The pore shape is strongly linked with the processing technique and some authors have linked changes in Poisson's ratio to changes in microstructure [53–55]. However, results of this study suggest that, in general, increase in porosity can cause the reduction of Poisson's ratio.

5. Conclusions

In this study Ti_2AlC and Ti_3SiC_2 foams have been processed successfully with controlled porosity and pore size using crystalline sugar powder as a space holder. This study shows that:

- The processing method employed can be reliably used to produced Ti_2AlC and Ti_3SiC_2 with acceptable phase stability. There are small variations in the phase composition of Ti_2AlC foams after sintering samples with and without space holder. For Ti_3SiC_2, decomposition of Ti_3SiC_2 into TiC is observed during sintering, which is more pronounced with increasing porosity. Mass loss measurements suggest that the phase changes are due the increase in the specific surface area, which favors Si vaporization. In the case of Ti_2AlC, increase in the amount of TiC, Ti_3AlC_2 and Al_2O_3 impurities after sintering are noticed and they were attributed to the partial decomposition of Ti_2AlC due to Al vaporization and some additional oxidation of the samples.
- The amount and type of porosity in the foams produced is consistent and can be controlled. The pore size distribution after sintering was found to be bimodal with micro-sized pores (microporosity) and macroporosity. The microporosity is confined to the cell walls and is due to incomplete densification during sintering. The macroporosity results from the removal of space holder. Increasing the amount of space holder leads to

increasing macroporosity. As the total amount of porosity increases, regardless of pore size, the cell walls become thinner and the micro-sized pores become interconnected and contribute to the open porosity. Neither the space holder amount nor the space holder size distribution affect significantly the size (EDC) of micro-sized pores.

- Elastic properties were determined for porosity values up to 71 vol% for Ti_2AlC and 69 vol% for Ti_3SiC_2. The exponential model, Hasselman model and CSM model were fitted to the experimental data over the whole range of porosity.
- For Ti_2AlC foams, the variations of Young's and shear moduli with porosity depends mostly on whether the porosity is open or closed. The model that best describes the elastic properties of Ti_2AlC foams over the whole range of porosity is the CSM.
- For Ti_3SiC_2 foams, a good fitting of the experimental data of Young's and shear moduli with all the models was obtained over the entire range of porosity.
- Poisson's ratio decreases with increasing porosity for both materials.
- The Young's, bulk and shear moduli were determined for foams with different pore size ranges for both Ti_2AlC and Ti_3SiC_2 foams. Porosity type in terms of open or closed porosity has a stronger influence on elastic properties than pore size distribution for both foam materials.

Acknowledgments

The authors would like to thank the funding provided for this research by the Regional Government of Madrid (Dir. Gral. Universidades e Investigación) through the project S2013/MIT-2862 (MULTIMAT-CHALLENGE-CM), the Spanish Government through the Ramón y Cajal contract RYC-2014-15014 and the project MAT2012-38650-C02-01, the Institute Alvaro Alonso Barba (IAAB) for funding for the research stay in Texas A&M University, and to Untied States of America - National Science Foundation through grants NSF-CMMI 1233792 and NSF-CMMI 1729350.

References

[1] M.W. Barsoum, The MN+1AXN phases: a new class of solids, Prog. Solid State Chem. 28 (2000) 201–281, https://doi.org/10.1016/S0079-6786(00)00006-6.
[2] M. Radovic, M.W. Barsoum, MAX phases: bridging the gap between metals and ceramics, Am. Ceram. Soc. Bull. 92 (2013) 20–27.
[3] M.W. Barsoum, T. Zhen, S.R. Kalidindi, M. Radovic, A. Murugaiah, Fully reversible, dislocation-based compressive deformation of Ti3SiC2 to 1GPa, Nat. Mater. 2 (2003) 107–111, https://doi.org/10.1038/nmat814.
[4] R. Benitez, W.H. Kan, H. Gao, M. O'Neal, G. Proust, M. Radovic, Room temperature stress-strain hysteresis in Ti2AlC revisited, Acta Mater. 105 (2016) 294–305, https://doi.org/10.1016/j.actamat.2015.12.004.
[5] R. Benitez, H. Gao, M. O'Neal, P. Lovelace, G. Proust, M. Radovic, Effects of microstructure on the mechanical properties of Ti2AlC in compression, Acta Mater. 143 (2018) 130–140.
[6] M.W. Barsoum, M. Radovic, Elastic and mechanical properties of the MAX phases, Annu. Rev. Mater. Res. 41 (2011) 195–227, https://doi.org/10.1146/annurev-matsci-062910-100448.
[7] A.G. Zhou, M.W. Barsoum, S. Basu, S.R. Kalidindi, T. El-Raghy, Incipient and regular kink bands in fully dense and 10 vol.% porous Ti2AlC, Acta Mater. 54 (2006) 1631–1639, https://doi.org/10.1016/j.actamat.2005.11.035.
[8] C.R. Bowen, T. Thomas, Macro-porous Ti2AlC MAX-phase ceramics by the foam replication method, Ceram. Int. 41 (2015) 12178–12185, https://doi.org/10.1016/j.ceramint.2015.06.038.
[9] Ziqi Sun, Ying Liang, Meishuan Li, Yanchun Zhou, Preparation of reticulated MAX-phase support with morphology-controllable nanostructured ceria coating for gas exhaust catalyst devices, J. Am. Ceram. Soc. 93 (2010) 2591–2597, https://doi.org/10.1111/j.1551-2916.2010.03776.x.
[10] M. Potoczek, E. Guzi de Moraes, P. Colombo, Ti2AlC foams produced by gel-casting, J. Eur. Ceram. Soc. 35 (2015) 2445–2452, https://doi.org/10.1016/j.jeurceramsoc.2015.03.015.
[11] Z.M. Sun, A. Murugaiah, T. Zhen, A. Zhou, M.W. Barsoum, Microstructure and mechanical properties of porous Ti3SiC2, Acta Mater. 53 (2005) 4359–4366, https://doi.org/10.1016/j.actamat.2005.05.034.
[12] É.P. Pechkovskii, S.A. Firstov, Structure and mechanical properties of porous titanosilicon carbide Ti3SiC2, Powder Metall. Met. Ceram. 42 (n.d.) 424–432. https://doi.org/10.1023/B:PMMC.0000004164.63420.14.
[13] S.A. Firstov, V.F. Gorban, I.I. Ivanova, E.P. Pechkovskii, Mechanical properties of porous Ti3SiC2/TiC, Ti3AlC2/TiC, and Ti4AlN3/TiN nanolaminates at 20 to 1300°C, Powder Metall. Met. Ceram. 49 (2010) 414–423, https://doi.org/10.1007/s11106-010-9252-2.
[14] S.A. Firstov, E.P. Pechkovsky, I.I. Ivanova, N.P. Brodnikovsky, V.F. Gorban, A.N. Demidik, High-temperature mechanical properties of powder metallurgy: porous lightweight titanium nanolaminates, High Temp. Mater. Process. 25 (2011) 47–58, https://doi.org/10.1515/HTMP.2006.25.1-2.47.
[15] L. Hu, R. Benitez, S. Basu, I. Karaman, M. Radovic, Processing and characterization of porous Ti2AlC with controlled porosity and pore size, Acta Mater. 60 (2012) 6266–6277, https://doi.org/10.1016/j.actamat.2012.07.052.
[16] C.L. Zhou, T.W.L. Ngai, L. Lu, Y.Y. Li, Fabrication and characterization of pure porous Ti3SiC2 with controlled porosity and pore features, Mater. Lett. 131 (2014) 280–283, https://doi.org/10.1016/j.matlet.2014.05.198.
[17] B. Velasco, E. Gordo, S.A. Tsipas, MAX phase Ti2AlC foams using a leachable space-holder material, J. Alloys Compd. 646 (2015) 1036–1042, https://doi.org/10.1016/j.jallcom.2015.05.235.
[18] B. Velasco, S.A. Tsipas, B. Ferrari, E. Gordo, MAX phase foams produced via powder metallurgy process using water soluble space holder, Powder Metall. 58 (2015) 95–99, https://doi.org/10.1179/0032589915Z.000000000226.
[19] L. Hu, I. Karaman, M. Radovic, Simple, inexpensive synthesis of damage-tolerant MAX phase foams, Am. Ceram. Soc. Bull. 92 (2013) 31–32.
[20] M. Fraczkiewicz, A.G. Zhou, M.W. Barsoum, Mechanical damping in porous Ti3SiC2, Acta Mater. 54 (2006) 5261–5270, https://doi.org/10.1016/j.actamat.2006.06.052.
[21] S. Amini, M.W. Barsoum, On the effect of texture on the mechanical and damping properties of nanocrystalline Mg-matrix composites reinforced with MAX phases, Mater. Sci. Eng. A 527 (2010) 3707–3718, https://doi.org/10.1016/j.msea.2010.01.073.
[22] A. Kontsos, T. Loutas, V. Kostopoulos, K. Hazeli, B. Anasori, M.W. Barsoum, Nanocrystalline Mg–MAX composites: mechanical behavior characterization via acoustic emission monitoring, Acta Mater. 59 (2011) 5716–5727, https://doi.org/10.1016/j.actamat.2011.05.048.
[23] L. Hu, M. O'Neil, V. Erturun, R. Benitez, G. Proust, I. Karaman, M. Radovic, High-performance metal/carbide composites with far-from-equilibrium compositions and controlled microstructures, Sci. Rep. 6 (2016) 35523, https://doi.org/10.1038/srep35523.
[24] L.J. Gibson, Michael F. Ashby, Cellular Solids, second ed., Cambridge state science series, 1999. http://www.cambridge.org/gf/academic/subjects/engineering/materials-science/cellular-solids-structure-and-properties-2nd-edition?format=PB. (Accessed 7 November 2016).
[25] H.-P. Degischer, B. Kriszt, Handbook of Cellular Metals: Production, Processing, Applications, Wiley-VCH, 2002.
[26] T. Marcu Puscas, M. Signorini, A. Molinari, G. Straffelini, Image analysis investigation of the effect of the process variables on the porosity of sintered chromium steels, Mater. Char. 50 (2003) 1–10, https://doi.org/10.1016/S1044-5803(01)00186-3.
[27] M. Radovic, E. Lara-Curzio, L. Riester, Comparison of different experimental techniques for determination of elastic properties of solids, Mater. Sci. Eng. Struct. Mater. Prop. Microstruct. Process. 368 (2004) 56–70, https://doi.org/10.1016/j.msea.2003.09.080.
[28] P. Gudlur, A. Forness, J. Lentz, M. Radovic, A. Muliana, Thermal and mechanical properties of Al/Al2O3 composites at elevated temperatures, Mater. Sci. Eng. A 531 (2012) 18–27, https://doi.org/10.1016/j.msea.2011.10.001.
[29] M. Radovic, M.W. Barsoum, A. Ganguly, T. Zhen, P. Finkel, S.R. Kalidindi, E. Lara-Curzio, On the elastic properties and mechanical damping of Ti3SiC2, Ti3GeC2, Ti3Si0.5Al0.5C2 and Ti2AlC in the 300–1573 K temperature range, Acta Mater. 54 (2006) 2757–2767, https://doi.org/10.1016/j.actamat.2006.02.019.
[30] R.M. Spriggs, Expression for effect of porosity on elastic modulus of polycrystalline refractory materials, particularly aluminum oxide, J. Am. Ceram. Soc. 44 (1961) 628–629, https://doi.org/10.1111/j.1151-2916.1961.tb11671.x.
[31] F.P. Knudsen, Effect of porosity on Young's modulus of alumina, J. Am. Ceram. Soc. 45 (1962) 94–95, https://doi.org/10.1111/j.1151-2916.1962.tb11089.x.
[32] D.P.H. Hasselman, On the porosity dependence of the elastic moduli of polycrystalline refractory materials, J. Am. Ceram. Soc. 45 (1962) 452–453, https://doi.org/10.1111/j.1151-2916.1962.tb11191.x.
[33] Z. Hashin, Elasticity of Ceramic Systems. Ceramic Microstructures '76: with Emphasis on Energy Related Applications, R. M. Fulrath and J. A. Pask, 1977, pp. 313–341.
[34] N. Ramakrishnan, V.S. Arunachalam, Effective elastic moduli of porous solids, J. Mater. Sci. 25 (n.d.) 3930–3937. https://doi.org/10.1007/BF00582462.
[35] N. Ramakrishnan, V.S. Arunachalam, Effective elastic moduli of porous ceramic materials, J. Am. Ceram. Soc. 76 (1993) 2745–2752, https://doi.org/10.1111/j.1151-2916.1993.tb04011.x.
[36] K.K. Phani, S.K. Niyogi, Young's modulus of porous brittle solids, J. Mater. Sci. 22 (n.d.) 257–263. https://doi.org/10.1007/BF01160581.
[37] J. Kováčik, Correlation between Young's modulus and porosity in porous materials, J. Mater. Sci. Lett. 18 (n.d.) 1007–1010. https://doi.org/10.1023/A:1006669914946.
[38] J. Kováčik, Correlation between shear modulus and porosity in porous materials, J. Mater. Sci. Lett. 20 (2001) 1953–1955.
[39] F. Cheng, S.-M. Kim, J.N. Reddy, Computational modeling of the plastic-damage behavior of porous MAX phase with aligned ellipsoid-like pores

under uniaxial compression, Int. J. Solid Struct. 63 (2015) 121–138, https://doi.org/10.1016/j.ijsolstr.2015.02.046.
[40] S. Amini, C. Ni, M.W. Barsoum, Processing, microstructural characterization and mechanical properties of a Ti2AlC/nanocrystalline Mg-matrix composite, Compos. Sci. Technol. 69 (2009) 414–420, https://doi.org/10.1016/j.compscitech.2008.11.007.
[41] W.K. Pang, I.M. Low, B.H. O'Connor, V.K. Peterson, A.J. Studer, J.P. Palmquist, In situ diffraction study of thermal decomposition in Maxthal Ti2AlC, J. Alloys Compd. 509 (2011) 172–176, https://doi.org/10.1016/j.jallcom.2010.09.019.
[42] W.K. Pang, I.M. Low, B.H. O'Connor, A.J. Studer, V.K. Peterson, Z.M. Sun, J.-P. Palmquist, Comparison of thermal stability in MAX 211 and 312 phases, J. Phys. Conf. Ser. 251 (2010), 012025, https://doi.org/10.1088/1742-6596/251/1/012025.
[43] C.B. Spencer, J.M. Córdoba, N. Obando, A. Sakulich, M. Radovic, M. Odén, L. Hultman, M.W. Barsoum, Phase evaluation in Al2O3 fiber-reinforced Ti2AlC during sintering in the 1300° C–1500° C temperature range, J. Am. Ceram. Soc. 94 (2011) 3327–3334.
[44] C. Racault, F. Langlais, R. Naslain, Solid-state synthesis and characterization of the ternary phase Ti3SiC2, J. Mater. Sci. 29 (n.d.) 3384–3392. https://doi.org/10.1007/BF00352037.
[45] Erdong Wu, E.H. Kisi, S.J. Kennedy, A.J. Studer, In situ neutron powder diffraction study of Ti[sub 3]SiC[sub 2] synthesis, J. Am. Ceram. Soc. 84 (2001) 2281.
[46] N.F. Gao, Y. Miyamoto, D. Zhang, On physical and thermochemical properties of high-purity Ti3SiC2, Mater. Lett. 55 (2002) 61–66, https://doi.org/10.1016/S0167-577X(01)00620-6.
[47] P. Eklund, C. Virojanadara, J. Emmerlich, L.I. Johansson, H. Högberg, L. Hultman, Photoemission studies of ${\mathrm{Ti}}_{3}\mathrm{Si}{\mathrm{C}}_{2}$ and nanocrystalline-TiC/amorphous-SiC nanocomposite thin films, Phys. Rev. B 74 (2006), 045417, https://doi.org/10.1103/PhysRevB.74.045417.
[48] J. Emmerlich, D. Music, P. Eklund, O. Wilhelmsson, U. Jansson, J.M. Schneider, H. Högberg, L. Hultman, Thermal stability of Ti 3 SiC 2 thin films, Acta Mater. 55 (2007) 1479–1488.
[49] T. El-Raghy, M.W. Barsoum, Processing and mechanical properties of Ti3SiC2: I, reaction path and microstructure evolution (vol 82, pg 2849, 1999), J. Am. Ceram. Soc. 83 (2000), 679–679.
[50] N. Tzenov, M.W. Barsoum, T. El-Raghy, Influence of small amounts of Fe and V on the synthesis and stability of Ti3SiC2, J. Eur. Ceram. Soc. 20 (2000) 801–806, https://doi.org/10.1016/S0955-2219(99)00166-1.
[51] T. El-Raghy, M.W. Barsoum, Diffusion kinetics of the carburization and silicidation of Ti3SiC2, J. Appl. Phys. 83 (1998) 112.
[52] J.C. Wang, Young's modulus of porous materials, J. Mater. Sci. 19 (n.d.) 801–808. https://doi.org/10.1007/BF00540451.
[53] H. Högberg, J. Emmerlich, P. Eklund, O. Wilhelmsson, J.P. Palmquist, U. Jansson, L. Hultman, Growth and property characterization of epitaxial MAX-phase thin films from the Tin+1(Si, Ge, Sn)Cn systems, Adv. Sci. Technol. 45 (2006) 2648–2655, https://doi.org/10.4028/www.scientific.net/AST.45.2648.
[54] S. Dubois, T. Cabioc'h, P. Chartier, V. Gauthier, M. Jaouen, A new ternary nanolaminate carbide: Ti3SnC2, J. Am. Ceram. Soc. 90 (2007) 2642–2644, https://doi.org/10.1111/j.1551-2916.2007.01766.x.
[55] M.B. Kanoun, M. Jaouen, Structure of the ternary carbide Ti 3 SnC 2 from ab initio calculations, J. Phys. Condens. Matter 20 (2008), 085211, https://doi.org/10.1088/0953-8984/20/8/085211.